Electronic Supplementary Material (ESI) for Chemical Communications.

Two-Component Supramolecular Metallogels with the Presence of Pt---Pt Metal–Metal Interactions

Zongchun Gao,[†] Peter A. Korevaar,[‡] Ruolei Zhong,[†] Zehong Wu,[†] and Feng Wang[†]*

† CAS Key Laboratory of Soft Matter Chemistry, iChEM (Collaborative Innovation Center of Chemistry for Energy Materials), Department of Polymer Science and Engineering, University of Science and Technology of China, Hefei, Anhui 230026 (P. R. China), E-mail: drfwang@ustc.edu.cn.

‡ Institute for Molecules and Materials, Radboud University, Heyendaalseweg 135, 6525 AJ Nijmegen, The Netherlands.

Supporting Information

1. Materials and Methods

Copper iodide (CuI) was reagent grade and used as received. [Pt(tpy)Cl](BF_4), 6-phenyl-2,2′-bipyridine platinum(II) chloride [(N^N^C)PtCl], compounds **2a**, **3**, and **4** were synthesized according to the previously reported procedures.[S1–S3] Other reagents and solvents were employed as purchased.

^{1}H NMR spectra were collected on Varian Unity INOVA-300 or INOVA-400 spectrometer with TMS as the internal standard. ^{13}C NMR spectra were recorded on Varian Unity INOVA-300 spectrometer at 75 MHz. MALDI-TOF measurements were recorded on a Bruker Autoflex Speed spectrometer with DCTB as the matrix. UV/Vis spectra were recorded on UV-1800 Shimadzu spectrometer. Steady-state emission spectra were recorded on FluoroMax-4 spectrofluorometer (Horiba Scientific) and analyzed with an Origin (v8.1) integrated software FluoroEssence (v2.2). Fluorescence lifetime data were acquired with 1MHz LED laser with the excitation peak at 455 nm (NanoLED-455). Lifetime data were analyzed with DataStation v6.6 (Horiba Scientific). Transmission electron microscope (TEM) images were performed on Tecnai G2 Spirit BioTWIN electron microscope (acceleration voltage: 120 kV). Rheological experiments were performed by the TA ARG2 stress-controlled rheometer with 40 mm parallel plate geometry. Gel sample was transferred onto the plate at 298 K. Oscillatory dynamic shear experiments were performed in the frequency range of 0.2–200 rad/s, using a constant strain (0.2%) determined with a strain sweep to lie within the linear viscoelastic regime.

For preparation of the co-assembled sample in solution: since either **2a** or **2b** is totally insoluble in apolar MCH/DCE (95 : 5, *v*/*v*) or decane/DCE (95 : 5, *v*/*v*), the "diluted stock solution" method is employed to prepare the co-assembled samples **1**/**2a** and **1**/**2b**.

*2. Self-assembly behavior of **1***

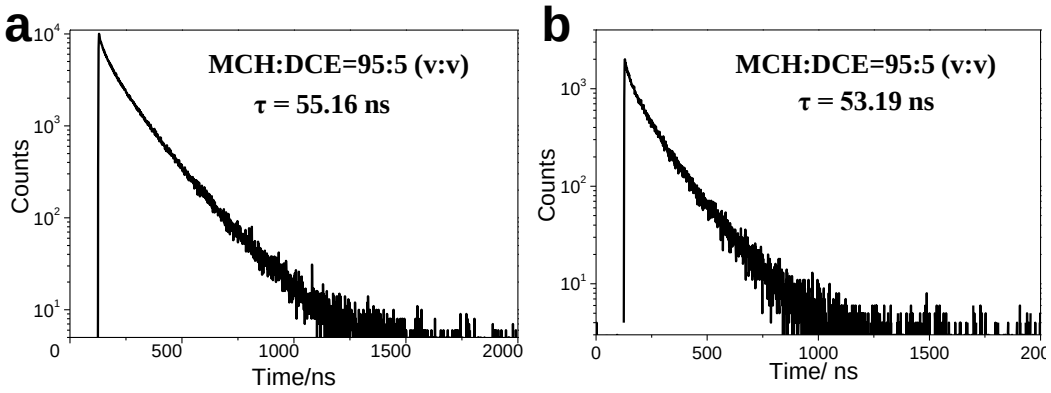

Figure S1. Photoluminescence lifetime decays of **1** [2×10^{-4} M in MCH/DCE (95 : 5, *v*/*v*)] at (a) 588 nm and (b) 612 nm. Accordingly, the averaged lifetime is determined to be 54.2 ns.

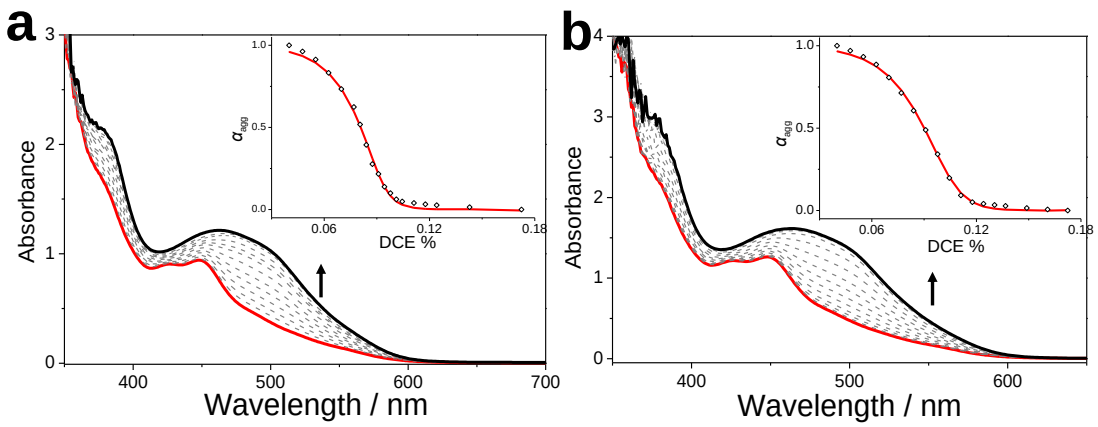

Figure S2. Solvent-dependent UV–Vis spectra of **1** at 303 K: (a) 0.30 mM; (b) 0.40 mM; in MCH/DCE (95 : 5, v/v). Arrows indicate the spectral changes upon increasing DCE fraction. Inset: α_{agg} as a function of DCE fraction for **1** (λ = 485 nm). Non-linear fitting of the normalized curve with the previously reported solvent-dependent equilibrium model.[S4]

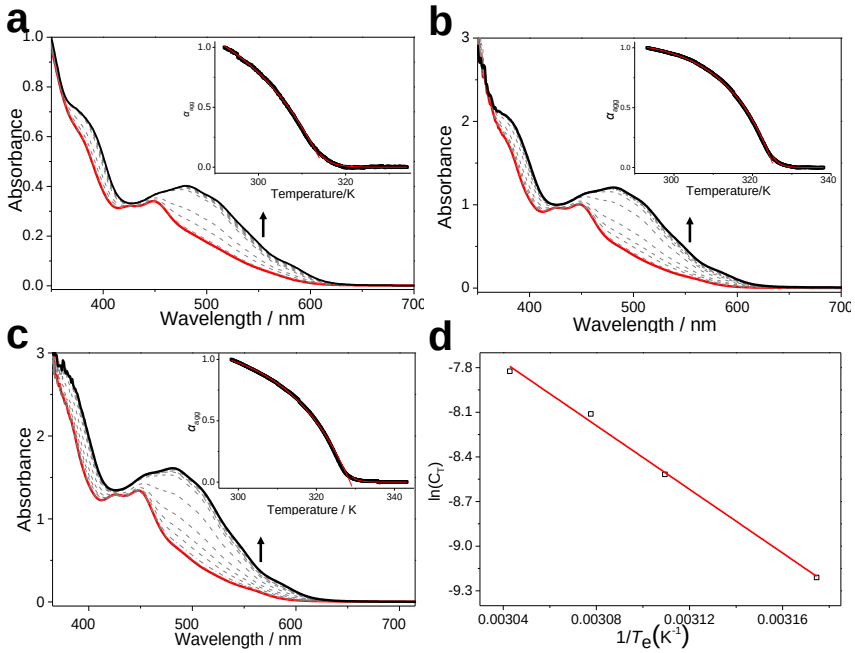

Figure S3. Temperature-dependent UV–Vis spectra of **1**: (a) 0.10 mM; (b) 0.30 mM; (c) 0.40 mM in MCH/DCE (95 : 5, v/v). Arrows indicate the spectral changes upon increasing temperature. Inset: α_{agg} as a function of temperature for **1** (λ = 485 nm). Non-linear fitting of the normalized curve with the Meijer–Schenning–Van-der-Schoot mathematical model affords the corresponding thermodynamic parameters (Table S1).[S5] (d) van't Hoff plot fitting and the corresponding thermodynamic values. The concentration was made dimensionless by dividing 1 M.

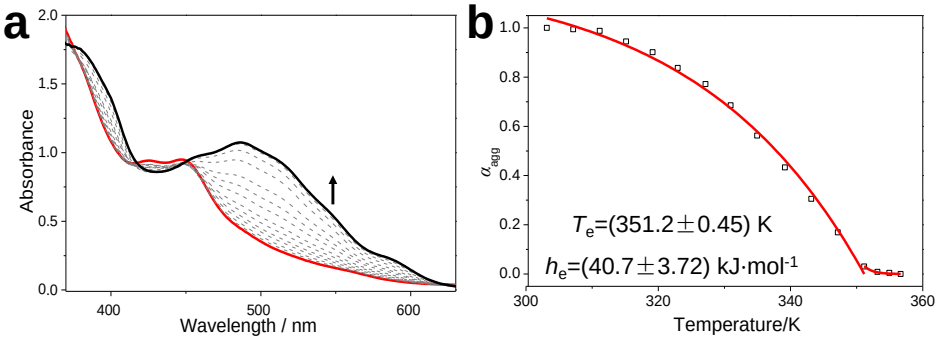

Figure S4. (a) Temperature-dependent UV–Vis absorption spectra of **1** (0.20 mM) in decane/DCE (95 : 5, *v*/*v*). Arrows indicate the spectral changes upon increasing temperature. (b) α_{agg} as a function of temperature for **1** (λ = 485 nm). Non-linear fitting of the normalized curve with the Meijer–Schenning–Van-der-Schoot mathematical model affords the corresponding thermodynamic parameters (Table S1).[S5]

Table S1. Thermodynamic parameters of **1** in MCH/DCE (95 : 5, *v*/*v*) and decane/DCE (95 : 5, *v*/*v*) obtained by fitting the temperature-dependent UV–Vis absorption data.

Solvent	Concentration [M]	T_e [K]	h_e [kJ mol^{-1}]
MCH/DCE=95:5	4.0 x 10^{-4}	328.64 ± 0.03	–56.7 ± 0.59
MCH/DCE=95:5	3.0 x 10^{-4}	324.89 ± 0.02	–67.0 ± 0.38
MCH/DCE=95:5	2.0 x 10^{-4}	321.60 ± 0.02	–61.5 ± 0.46
MCH/DCE=95:5	1.0 x 10^{-4}	315.00 ± 0.04	–52.5 ± 0.82
Decane/DCE=95:5	2.0 x 10^{-4}	351.23 ± 0.45	–40.7 ± 3.72

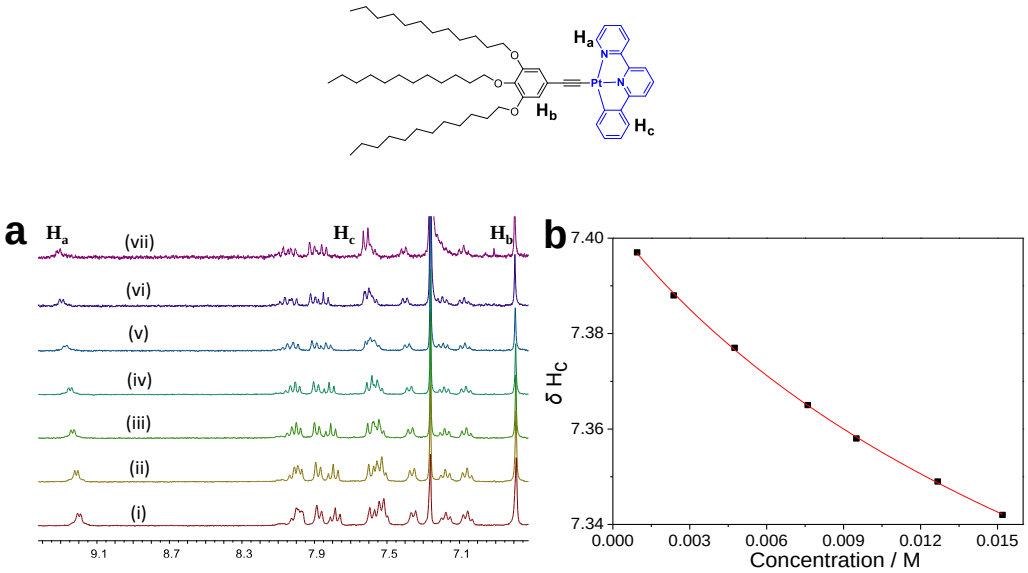

Figure S5. (a) Partial ^{1}H NMR spectra (300 MHz, $CDCl_3$, 298 K) of **1** at different monomer concentrations (from 15.2 mM of i to 0.95 mM of viii). (b) Chemical resonances changes of H_c on **1**. The aromatic protons on the main ligand show upfield shifts upon increasing the concentration, suggesting the involvement of π-π stacking interactions. By treating the collected chemical shift changes of proton H_c with the nonlinear curve-fitting equation, the association constant (K_a) value of **1** is determined to be (15.8 ± 2.2) M^{-1} in *d*-chloroform.

*3. Self-assembly behavior of **2a***

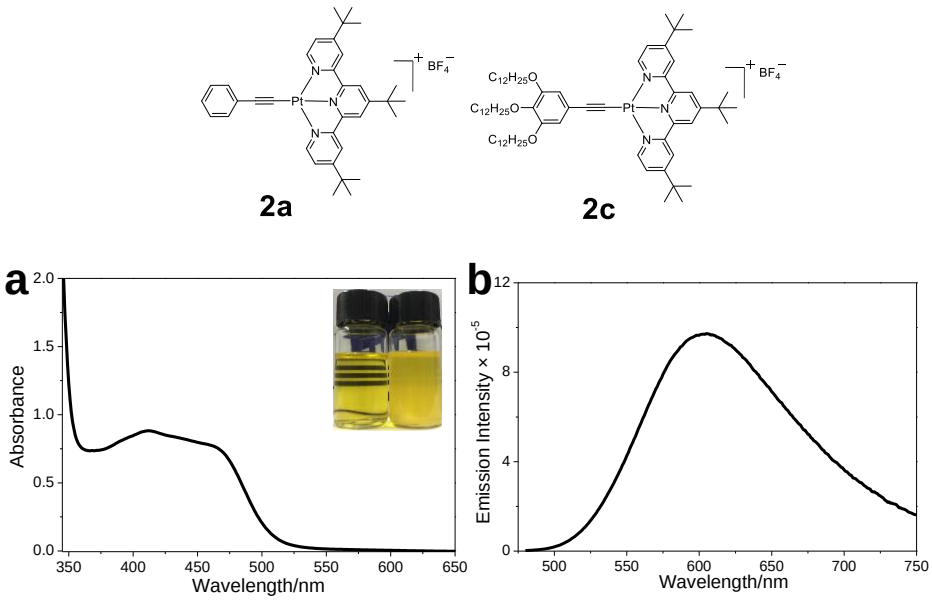

Figure S6. (a) UV–Vis absorption and (b) fluorescent spectra of **2a** in DCE. Inset: images of the solution colors of **2a** in DCE and MCH/DCE (95 : 5, *v*/*v*).

Since **2a** is insoluble and forms yellow suspension in apolar solvent, the model compound **2c** is further employed to study the spectroscopic behaviors.

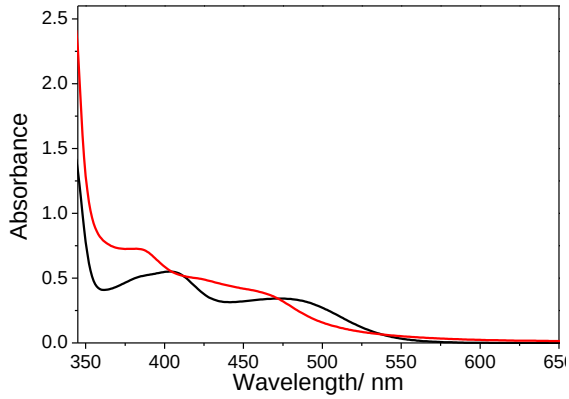

Figure S7. (a) UV–Vis absorption of **2c** in DCE (black line) and MCH/DCE (95 : 5, *v*/*v*) (red line). For **2c**, the maximum MLCT/LLCT absorption band is located at 483 nm in DCE. When switching the solvent to apolar MCH/DCE (95 : 5, *v*/*v*), those band displays a hypochromic shift (λ_{max}= 467 nm). Hence, it is apparent that the newly-formed spectroscopic bands of **1**/**2a** (560–800 nm, Figure 2a in the main text) are not originated from the **2a** self-assembly process.

*4. Co-assembly behaviors of complexes **1/2a** and **1/2b***

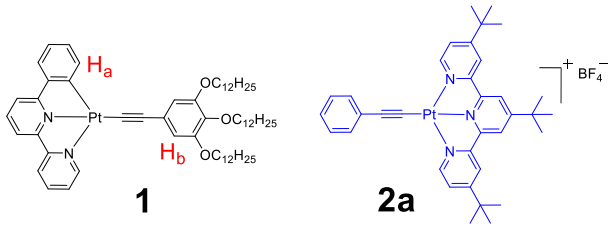

^{1}H NMR titration experiments were performed for complex **1**/**2a**. In detail, the initial concentration of **1** was kept constant at 2.00 mM, while concentration of **2a** was systematically varied. Treatment of the collected chemical shifts on **1** *vs* the concentration of guest (C_A) with a non-linear least-squares curve-fitting equation affords the association constants. Specifically, for 1 : 1 host/guest complexation, the binding constants are calculated according to the following equation:

$$\delta = \delta_0 + \frac{\delta_{lim}-\delta_0}{2C_0}\left[C_0 + C_A + \frac{1}{K_a} - \left[\left(C_0 + C_A + \frac{1}{K_a}\right)^2 - 4C_AC_0\right]^{1/2}\right] \quad \text{(Equation S1)}$$

δ_0 and δ are the chemical shifts for a selected host proton with and without the presence of the guest, respectively. [C_0] is the total concentration of the host, whilst [C_A] is the concentration of the guest. δ_{lim} is the limiting value of chemical shifts for a selected host proton with the presence of excess guest. K_a is the binding constant.

In terms of **1**/**2a**, K_a value is determined to be (72.5 ± 14.5) M^{-1} in $CDCl_3$, by nonlinear curve-fitting of the collected ^{1}H NMR resonances of H_a and H_b (Figure S8b).

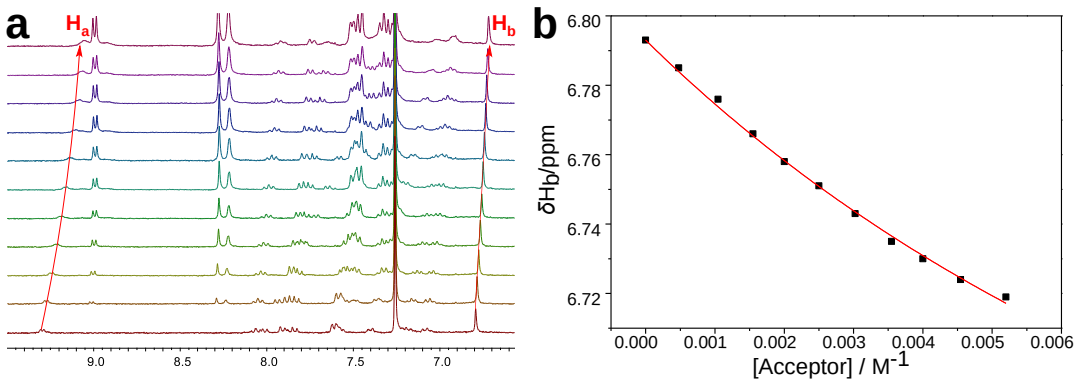

Figure S8. (a) ^{1}H NMR titration spectra (300 MHz, $CDCl_3$, 298 K) of **1** at the concentration of 2.00 mM upon progressive addition of **2a**. (b) Chemical resonances change for protons H_b on **1** and the nonlinear curve fittings. The aromatic protons on **1** display upfield shifts upon addition of **2a**, suggesting the involvement of donor–acceptor CT interactions.

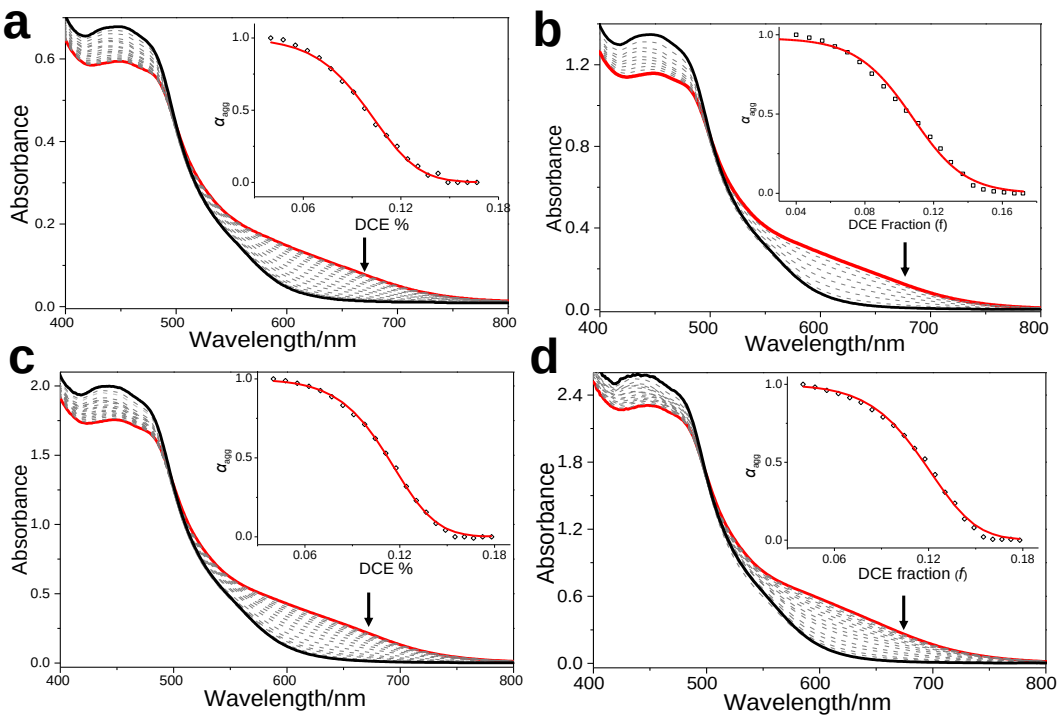

Figure S9. Solvent-dependent UV–Vis absorption spectra of **1/2a** at 303 K:(a) 0.10 mM, (b) 0.20 mM, (c) 0.30 mM and (d) 0.40 mM in MCH/DCE (95 : 5, *v*/*v*). Arrows indicate the spectral changes upon increasing DCE fraction. Inset: α_{agg} as a function of DCE fraction for **1/2a** (λ = 620 nm). Non-linear fitting of the normalized curve with the previously reported solvent-dependent equilibrium model.[S4]

Table S2. Thermodynamics of 1 and 1/2a assembling processes

Complex	σ	m (kJ/mol)	ΔG_0 (kJ/mol)	$\Delta G_{f=0.05}$ (kJ/mol)
1 [a]	0.004 ± 0.002	120 ± 4	–31.6 ± 0.3	–25.6 ± 0.1
1/2a [a]	1.0	177 ± 9	–39.1 ± 0.6	–30.1± 0.3
1/2a [b]	1.0	40.5 ± 0.5	–35.7 ± 0.4	–33.7± 0.4

(a) in DCE/MCH mixture. (b) in DCE/decane mixture.

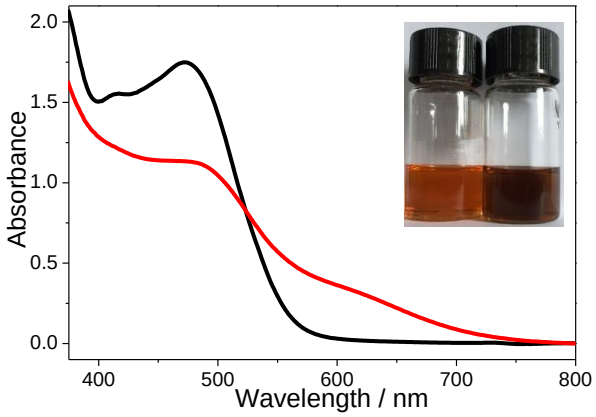

Figure S10. (a) UV–Vis absorbance spectra of a 2 : 1 mixture of **1** and **2b** ($c = 2 \times 10^{-4}$ M for **1**) in MCH/DCE (95 : 5, *v*/*v*) (red line) and DCE (black line). **1**/**2b** display similar UV–Vis spectra to those of **1**/**2a**, indicating that the alkyl crosslinking unit exerts minor effect on non-covalent complexation behaviors. Inset: images of the solution colors of **1**/**2a** in DCE and MCH/DCE (95 : 5, *v*/*v*).

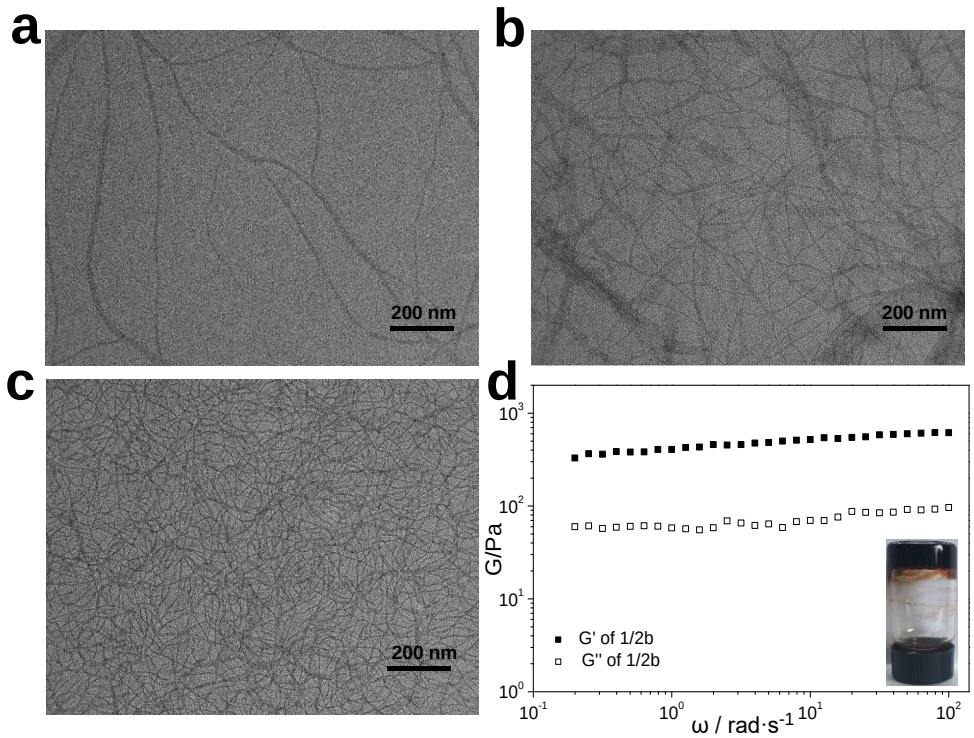

Figure S11. TEM image of (a) **1**, (b) **1**/**2a** and (c) **1**/**2b** on a carbon coated copper grid. (d) Storage modulus (G') and loss modulus (G'') values of the gels derived from **1**/**2b** in MCH/DCE (95 : 5, *v*/*v*). Inset: photographs of gel from **1**/**2b**.

*5. Synthetic routes to monomers **1** and **2b***

*5.1 Synthesis of monomer **1***

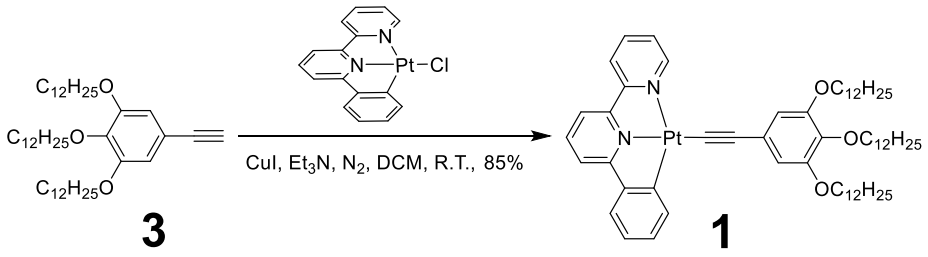

3 **1**

Compound **3** (393 mg, 0.60 mmol), [(N^N^C)Pt]Cl (230 mg, 0.50 mmol), CuI (9.50 mg, 0.05 mmol) and NEt_3 (1.5 mL) were dissolved in 30 mL of CH_2Cl_2, and stirred at room temperature for 12 hours. The mixture was evaporated under reduced pressure, and the residue was purified by column chromatography (alumina, CH_2Cl_2 as the eluent) to afford **1** as a red solid (460 mg, 85%). ^{1}H NMR (300 MHz, $CDCl_3$, 298K) δ (ppm): 9.18 (d, J = 5.2 Hz, 1H), 8.04 (dd, J = 21.1, 5.6 Hz, 1H), 7.97 (d, J = 7.8 Hz, 1H), 7.87 (d, J = 7.9 Hz, 1H), 7.78 (t, J = 8.0 Hz, 1H), 7.58 (d, J = 7.9 Hz, 1H), 7.51 (t, J = 7.0 Hz, 2H), 7.34 (d, J = 7.4 Hz, 1H), 7.17 (t, J = 7.0 Hz, 1H), 7.05 (t, J = 7.4 Hz, 1H), 6.79 (s, 2H), 4.07 – 3.87 (m, 6H), 1.79 (dd, J = 14.1, 6.8 Hz, 6H), 1.46 (s, 6H), 1.26 (s, 48H), 0.86 (dd, J = 6.8, 3.2 Hz, 9H).^{13}C NMR (75 MHz, $CDCl_3$, 298K) δ (ppm): 165.53, 157.95, 154.37, 152.65, 151.67, 146.69, 142.31, 138.62, 136.93, 131.46, 127.39, 124.39, 123.66, 123.51, 122.66, 118.35, 117.76, 110.40, 106.60, 103.32, 73.52, 69.07, 31.94, 30.38, 29.78, 29.72, 29.68, 29.48, 29.41, 29.38, 26.17, 22.70, 14.12. HRESIMS: m/z calcd for $[M + K]^+$, 1118.6080; found 1118.6012, error 6.08 ppm.

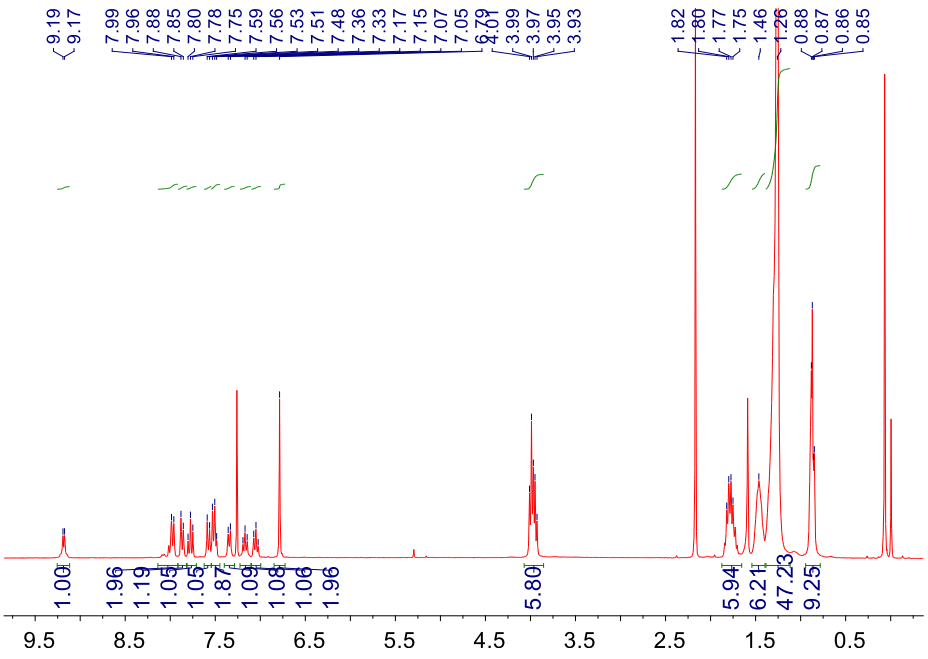

Figure S12. ^{1}H NMR spectrum (300 MHz, $CDCl_3$, 298 K) of **1**.

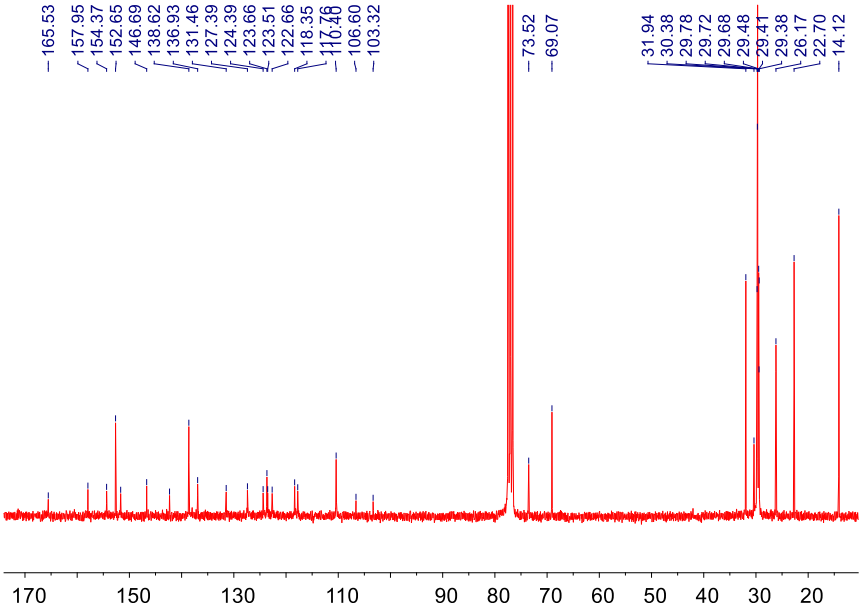

Figure S13. ^{13}C NMR spectrum (75 MHz, $CDCl_3$, 298 K) of **1**

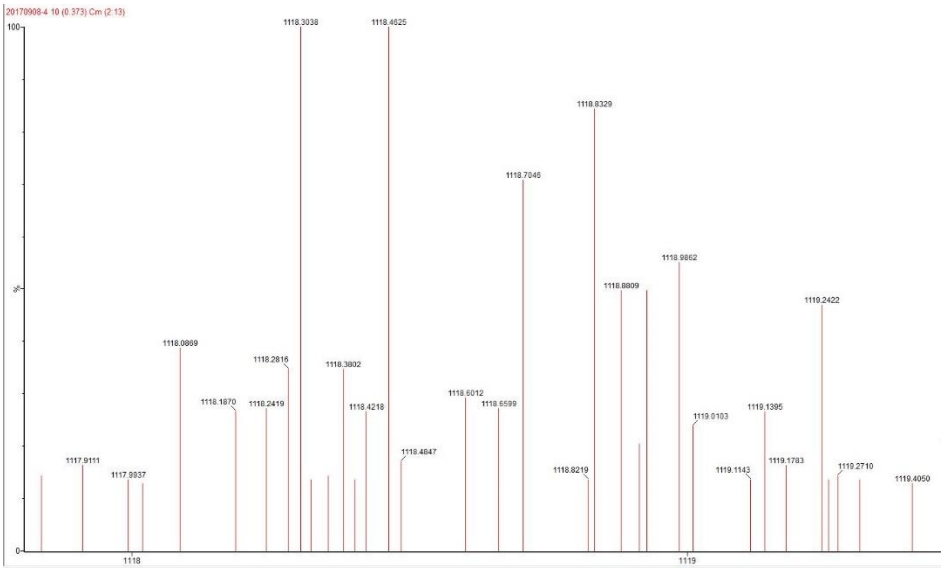

Figure S14. Electrospray ionization spectrum of **1**.

*5.2 Synthesis of **2b***

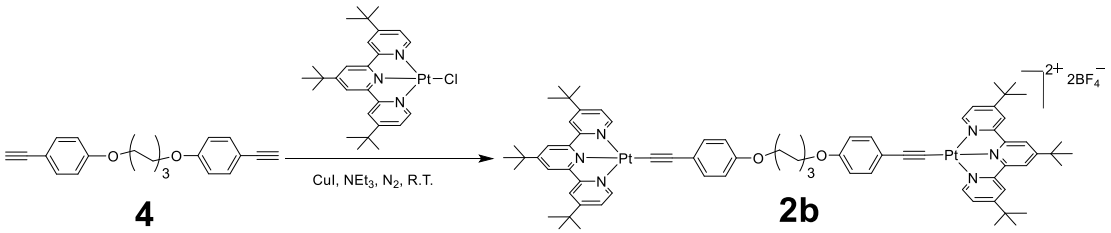

[Pt(tpy)Cl](BF$_4$) (432 mg, 0.60 mmol), compound **4** (80.0 mg, 0.25 mmol), CuI (7.60 mg, 0.04 mmol) and NEt$_3$ (1.5 mL) were dissolved in 30 mL of CH_2Cl_2, and stirred at room temperature for 24 hours. The mixture was evaporated under reduced pressure, and the residue was purified by column chromatography (alumina, CH_3OH/CH_2Cl_2, 100 : 1 *v*/*v* as the eluent) to afford **2b** as a red solid (388 mg, 92%). ^{1}H NMR (300 MHz, $CDCl_3$, 298K) δ (ppm): 9.15 (d, J = 6.0 Hz, 4H), 9.01 (s, 4H), 8.90 (d, J = 1.4 Hz, 4H), 7.57 (dd, J = 6.0, 1.7 Hz, 4H), 7.43 (d, J = 8.6 Hz, 4H), 6.85 (d, J = 8.7 Hz, 4H), 4.00 (t, J = 6.4 Hz, 4H), 1.84 (s, 4H), 1.66 (s, 18H), 1.52 (s, 40H). ^{13}C NMR (75 MHz, $CDCl_3$, 298K) δ (ppm): 168.92, 167.58, 159.04, 158.03, 153.88, 133.09, 124.89, 124.16, 122.49, 118.73, 114.35, 104.32, 95.04, 67.91, 37.85, 36.62, 30.83, 30.39, 29.19, 25.87. HRESIMS: *m*/*z* calcd for $[M - 2BF_4]^{2+}$, 754.3210; found 754.3203, error 0.93 ppm.

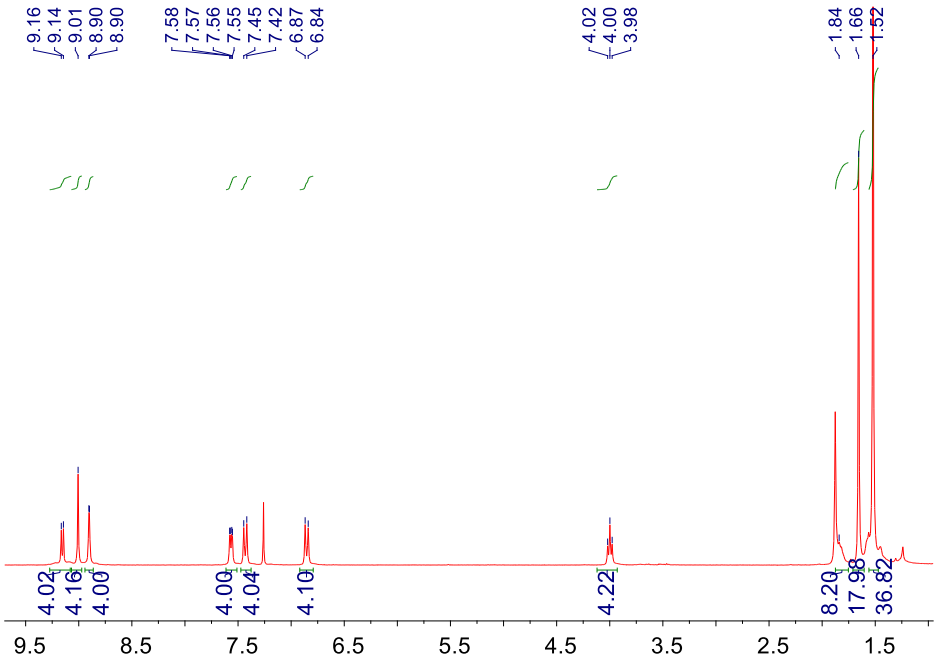

Figure S15. ^{1}H NMR spectrum (300 MHz, $CDCl_3$, 298 K) of **2b**.

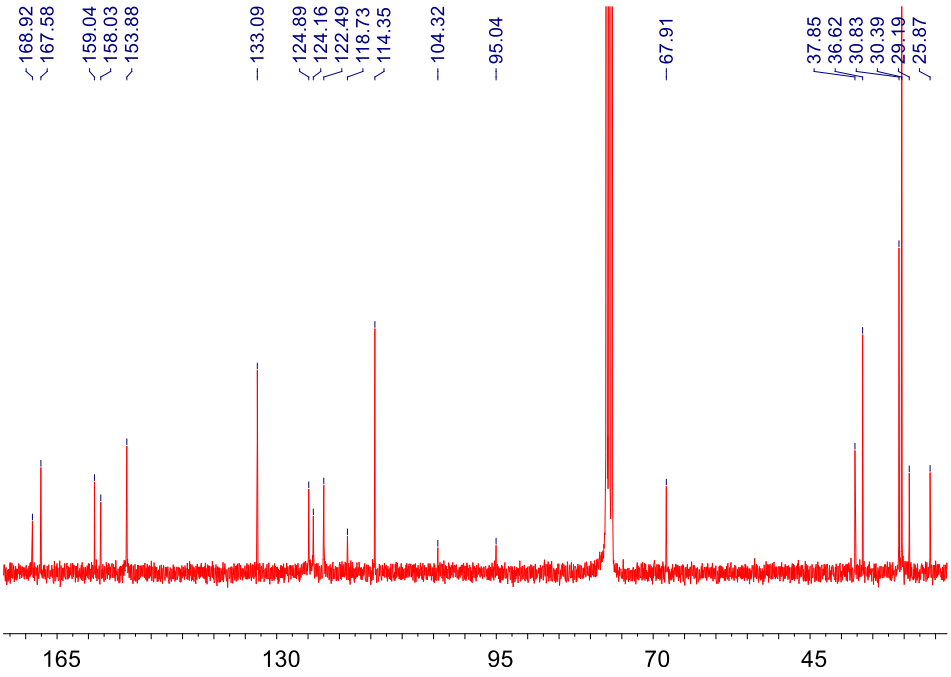

Figure S16. ^{13}C NMR spectrum (75 MHz, $CDCl_3$, 298 K) of **2b**.

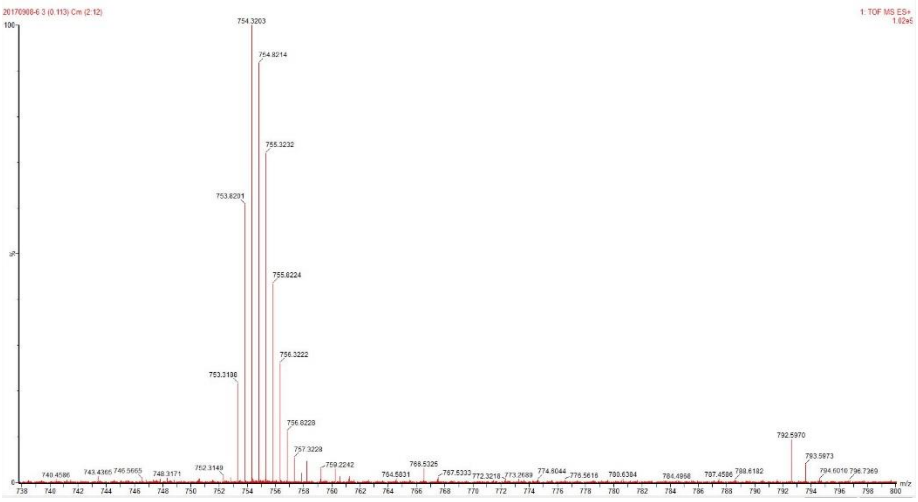

Figure S17. Electrospray ionization spectrum of **2b**.

6. Mathematical curve fitting of the assembling process

In terms of **1**, it adopts cooperative mechanism for the supramolecular assembling process. To acquire the detailed thermodynamic parameters for the self-assembly process, Meijer–Schenning–Van-der-Schoot model has been employed to fit the melting curves.[S3,S5] In detail, a non-sigmoidal curve can be obtained by plotting the fraction of aggregated species (α_{agg}) against temperature at 485 nm on the basis of temperature-dependent UV–Vis absorption spectra experiments. The supramolecular polymerization can be divided into two separated steps: the nucleation and elongation regimes. In the elongation regime, the fraction of aggregated molecules φ_n is described by Eq. S1:

$$\varphi_n = \varphi_{SAT}\{1 - exp[(-h_e) \times (T - T_e)/(R \times T_e^2)]\} \quad \text{(Eq. S1)}$$

In this equation, h_e denotes the molecular enthalpy release due to the non-covalent supramolecular polymerization, T and T_e stand for the absolute temperature and elongation temperature, respectively. R represents the universal gas constant. φ_{SAT} is a parameter that is introduced to prevent the relation φ_n/φ_{SAT} surpassing the value of one.

In the nucleation regime, it means that at temperatures below the elongation temperature T_e. φ_n is described by Eq. S2:

$$\varphi_n = {K_a}^{1/3} \times exp\left[\left(2/3K_a^{-1/3} - 1\right) \times h_e \times (T - T_e)/(R \times {T_e}^2)\right] \quad \text{(Eq. S2)}$$

K_a is the dimensionless equilibrium constant for the nucleation step at T_e. It is apparent that the data points are accurately fitted over the whole temperature range.

Depending on Eq. 1 and 2 in the main text, similar fitting process can be performed for the solvent-dependent UV-Vis experiments *via* Matlab R2016a software.

REFERENCES:

S1. W. Lu, B.-X. Mi, M. C. W. Chan, Z. H., C.-M. Che, N. Zhu and S.-T. Lee, *J. Am. Chem. Soc.*, 2004, **126**, 4958.

S2. Y.-K. Tian, Y.-G. Shi, Z.-S. Yang and F. Wang, *Angew. Chem. Int. Ed.* 2014, **53**, 6090.

S3. Z. Gao, Z. Li, Z. Gao and F. Wang, *Nanoscale*, 2018, **10**, 14005.

S4. P. A. Korevaar, C. Schaefer, T. F. A. de Greef and E. W. Meijer, *J. Am. Chem. Soc*., 2012, **134**, 13482.

S5. P. Jonkheijm, P. van der Schoot, A. P. H. J. Schenning and E. W. Meijer, *Science*, 2006, **313**, 80.